BJR

Received: 24 November 2015 | Revised: 3 February 2016 | Accepted: 2 March 2016

http://dx.doi.org/10.1259/bjr.20150988

Cite this article as:
Miki K, Mori S, Hasegawa A, Naganawa K, Koto M. Single-energy metal artefact reduction with CT for carbon-ion radiation therapy treatment planning. *Br J Radiol* 2016; **89**: 20150988.

FULL PAPER

Single-energy metal artefact reduction with CT for carbon-ion radiation therapy treatment planning

KENTARO MIKI, PhD, SHINICHIRO MORI, PhD, AZUSA HASEGAWA, MD, KENSUKE NAGANAWA, MD and MASASHI KOTO, MD

Research Center for Charged Particle Therapy, National Institute of Radiological Sciences, Chiba, Japan

Address correspondence to: Dr Kentaro Miki
E-mail: *miki.kentaro@qst.go.jp*

Objective: One approach to improving image quality of CT is to use metal artefact reduction image processing, such as single-energy metal artefact reduction (SEMAR). To quantify the impact of image correction on the quality of carbon-ion dose distribution, treatment planning using SEMAR was evaluated.
Methods: Using a head phantom into which metal screws could be inserted, we acquired standard planning CT images. We calculated dose distributions using phantom images with and without metal added, and with and without SEMAR. Hounsfield unit (HU) and dose distribution variation of these images with and without SEMAR were measured using metal-free image subtraction. We similarly analysed the image data sets of two patients with head and neck cancer who had dental implants.
Results: HU difference between metal-containing images and metal-free images without and with SEMAR were -79.5 ± 97.2 HU and -1.4 ± 19.5 HU on severe artefact area, respectively. The range of dose distribution difference from the prescribed dose between uncorrected and SEMAR-corrected images varied from −19.5% to −3.4% within planning target volume (PTV). PTV-D_{95} (%) for uncorrected and SEMAR-corrected image data were 82.4% and 95.4%, respectively. For data in patients with metal dental work, PTV-D_{95} (%) for uncorrected and SEMAR-corrected data were 92.2% and 92.5% (Patient 1), and 90.9% and 95.7% (Patient 2), respectively.
Conclusion: SEMAR algorithm shows promise in improving CT image quality and in ensuring an accurate representation of dose distribution.
Advances in knowledge: SEMAR may improve treatment accuracy without the need for dental implant extraction in patients with head and neck cancer.

INTRODUCTION

CT, which provides radiation attenuation information and calculates tissue density, is essential for treatment planning in complicated image-guided therapies using gamma rays and particle beams.[1] Artefacts in the CT image may affect dose distributions in the treatment plan. Metallic materials highly attenuate X-rays, causing artefacts due to both "photon starvation" and "beam hardening" along the X-ray beam path.[2] Examples are high-density dental implants, fiducial markers or hip prostheses. These generate metal artefact, which alters Hounsfield unit (HU) values,[3] resulting in an inaccurate dose distribution estimate. Compared with photon beam therapy, range of particle beam would be more sensitive to variation of water-equivalent path length (WEPL). Therefore, range uncertainty due to altered HUs on planning CT image needs to care especially particle beam therapy. Moreover, most of carbon-ion facilities do not equip a rotating gantry,[4] resulting in the limitation of irradiation beam angle. Artefact would be an additional limitation of beam angle selection in the treatment planning. In the case of head and neck cancer treatment, one of the main issues is the artefact from dental implants. Before acquiring a planning CT image, dental implants located close to the tumour are often removed to reduce the influence of metal artefact, causing patient discomfort.

In order to reduce the metal artefact from CT image in clinical use, several studies have introduced different approaches. These mainly involve manipulating X-ray energies, such as dual-energy acquisition techniques,[5] high-energy X-rays[6,7] and image processing, such as iterative reconstruction methods[8–10] or interpolation of metal object.[11–16] The majority of image processing approach treats the projections on metal objects which were segmented from sinograms or images as a corrupt or missing data. In the iterative reconstruction methods, the missing data are ignoring or reducing statistical contributions from image reconstruction calculation.[8–10] These methods improve image quality in patients wearing metal objects; however, they are computationally much more expensive

than standard filtered back projection method. In the interpolation of metal object methods, segmented missing data are interpolated by synthetic projections. One of the first completion methods used was linear interpolation.[11] Based on this approach, more number of advanced techniques were proposed, such as cubic spline interpolation,[12] wavelet coefficient interpolation[13] and inpainting techniques to obtain a better visualization.[14–16] Generally, interpolation approach compensates missing data and improves image quality with lower computational overhead compared with iterative reconstruction. Recently, these metal artefact reduction algorithms were implemented in commercial CT scanners for clinical practice.

Single-energy metal artefact reduction (SEMAR®, Toshiba Medical Systems, Otawara, Japan) is one of the metal artefact reduction algorithms. Although it has a higher computation cost than that of conventional image reconstruction, it can be applied to data after acquisition, facilitating its implementation into the routine workflow. While improvements in soft tissue visibility using SEMAR have been reported,[17,18] its use in radiation treatment planning has not been described. Since SEMAR changes HUs, its accuracy in quantifying actual lesions needs to be confirmed before using it in clinical treatment. We evaluated HU accuracy with and without SEMAR and compared the predicted dose distributions using an anthropomorphic head phantom with varying amounts of inserted metal, as well as patient CT data.

METHODS AND MATERIALS

Single-energy metal artefact reduction

The projection of passing through on the metallic materials is highly attenuated, which results in corrupt or missing projection data. SEMAR is a raw data-based algorithm that reduces metal artefact by applying linear interpolation to repeating forward and back projection processes. Gondim Teixeira et al[17] introduced the SEMAR calculation steps. First, metal densities in the original CT image are segmented by HU threshold. Then, the segmented metal image is forward projected to trace the metal's path on the sinogram of the raw data. The metal's path is defined by linear interpolation, using the values registered by adjacent channels at each angular position.[19] The linearly interpolated raw data are reconstructed to generate an image with the metal objects removed (second-pass image). The second-pass image is classified by HU thresholds for air, water and bone (tissue-class modelling,[20]) which are forward projected onto the metal's path. The tissue-classified forward projection is linearly integrated to the interpolated raw data and reconstructed again to obtain a third-pass image. Finally, the segmented metal CT image is added onto the third-pass image to obtain the final corrected image.

Phantom study

Data acquisition

Two CT data sets of an anthropomorphic head phantom were acquired using a 320-slice CT (Aquilion ONE Vision edition®, Toshiba Medical Systems), one set with the phantom containing inserted metal screws of 6-mm diameter and 8-mm length and the second without added metal. CT scan conditions were 120-kV tube voltage, 450-mA tube current, 1.0 s per rotation, slice collimation of 280 × 0.5 mm and volumetric scan mode. Reconstruction conditions were a 1.0-mm slice thickness using the iterative reconstruction algorithm adaptive iterative dose reduction 3D (AIDR3D),[21–23] with or without SEMAR. The convolution kernel was the standard body (FC13).

Image quality evaluation

Images of the phantom with the inserted metal screws processed with and without SEMAR were evaluated. The number of inserted screws was varied from zero to three. After selecting images containing metal artefact, we placed 7-mm regions of interest (ROIs) on areas with little or severe artefact (see red circles in Figure 1) and calculated the mean and standard deviation of HU values within these ROIs.

Dose distribution evaluation

Dose distribution was calculated with the treatment planning system (TPS) in using clinical practice in our facility. It was designed reflecting the physical and biological characteristics of carbon-ion beam to provide accurate relative biological effectiveness (RBE).[24–27] Carbon-ion irradiation was performed by delivering the dose in beam spots. The beam range was changed using a hybrid depth scanning technique, which consists of the combination of a synchrotron with 11 distinct energies for steps of 30 mm and a range shifter for WEPL steps of 3 mm.[28] Beam spot and beam weight optimization were performed using the TPS[29] for the data sets of the phantom including the screws with and without SEMAR. To calculate the dose distribution of SEMAR-uncorrected optimized treatment plans on the artefact-corrected images, beam spots and beam weights were optimized to the uncorrected images, and then the dose distribution was calculated on the artefact-corrected images. Dose differences were obtained by subtracting the SEMAR-corrected dose distribution from the SEMAR-uncorrected dose distribution. Planning target volume (PTV) was placed on the dark artefact band. Dose of 57.6 Gy (RBE) was delivered to achieve the median PTV to the prescribed dose from two different beam angles (0° and 90° in eight and four fractions). A single uniform field optimization was performed. Dose was represented as RBE-weighted absorbed dose [Gy (RBE)], which were defined as the absorbed dose of carbon ion multiplied by RBE.[30]

Patient study

Data acquisition

We conducted a treatment planning study with the data sets of two patients with dental implants who had head and neck cancer. As is routine, the patient was immobilized on the treatment couch with an immobilization device. CT was performed with tube voltage of 120 kV and tube current of 280 mA for Patient 1 and 220 mA for Patient 2, 1.5 s of rotation time, slice collimation of 280 slices × 0.5 mm, in volumetric scan mode. Reconstruction conditions were 1.0 mm slice thickness, AIDR3D applied, with and without SEMAR. The convolution kernel was the standard body (FC13).

Dose distribution evaluation

The contours of PTV or organs at risk (OARs) used for this study were copied from the clinical treatment plan. Since the original PTV location did not have an artefact in Patient 2, it was

Figure 1. The metal artefact images of head phantom with 1–3 screws without single-energy metal artefact reduction (SEMAR) (a–c) and with SEMAR (d–f). 7-mm regions of interest placed on areas with severe or no artefact (red circles). For colour image see online.

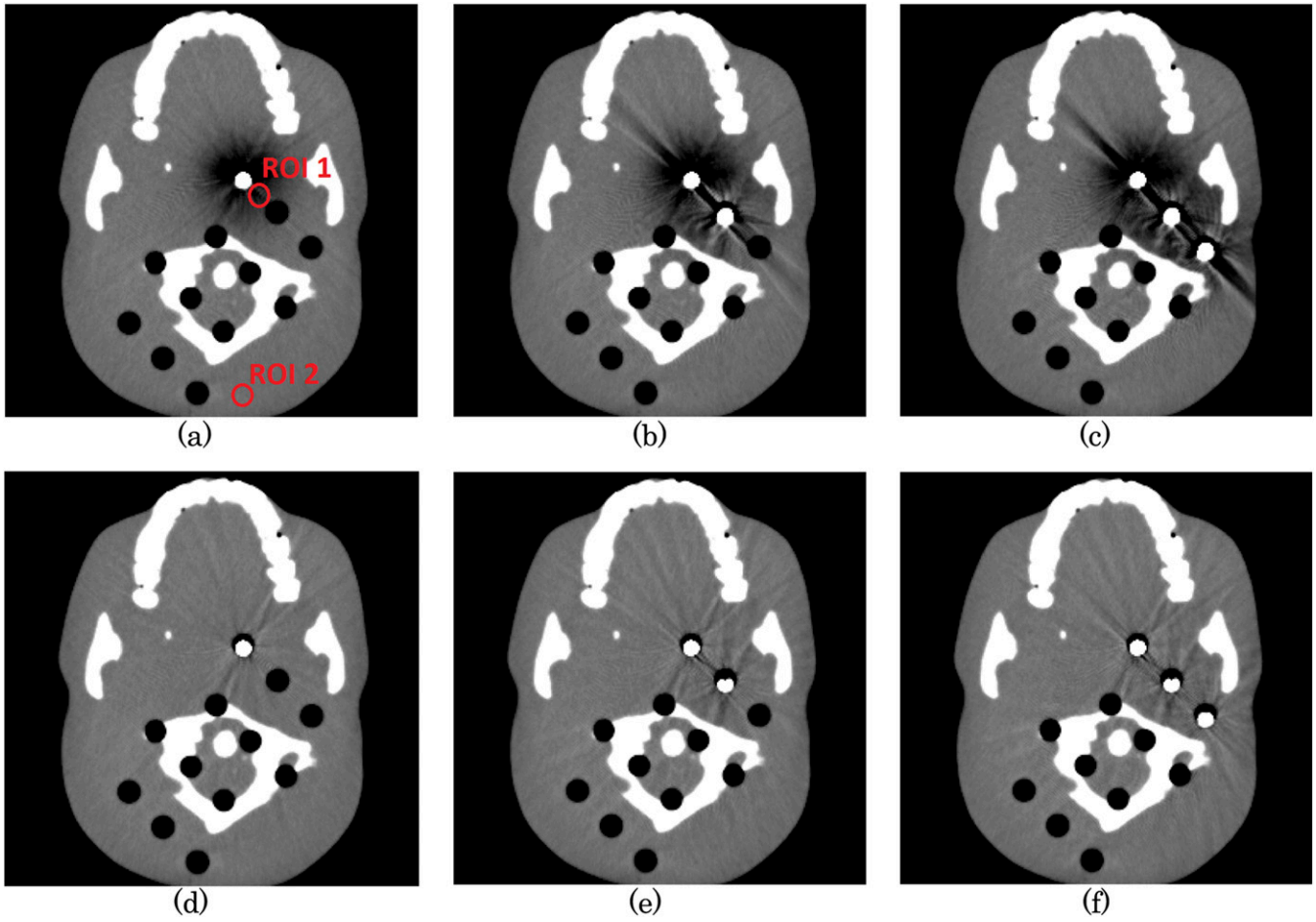

enlarged by 3 mm to confirm the SEMAR correction clearly in this study. The prescribed dose of 57.6 Gy (RBE) was delivered to PTV from two different beam angles (30° and 270° in eight and four fractions for Patient 1; 345° and 270° in eight and four fractions for Patient 2). Beam spot was optimized to an uncorrected image, and the dose distribution was calculated on the artefact-corrected images with SEMAR. The dose was compared between dose distributions of uncorrected and

Table 1. Mean, standard deviation (SD), maximum and minimum of Hounsfield unit (HU) of head phantom on regions of interest (ROIs) 1 and 2

ROI	Number of metal screws	Without SEMAR			With SEMAR		
		Mean ± SD (HU)	Min (HU)	Max (HU)	Mean ± SD (HU)	Min (HU)	Max (HU)
ROI 1	0	20.8 ± 6.3	−2	43	20.8 ± 6.3	−2	43
	1	5.6 ± 48.2	−189	95	19.4 ± 14.0	−33	82
	2	−31.3 ± 86.9	−695	187	18.6 ± 18.0	−82	95
	3	−58.7 ± 97.0	−768	289	19.4 ± 18.5	−88	98
ROI 2	0	8.5 ± 5.5	−8	28	8.5 ± 5.5	−8	28
	1	5.9 ± 6.4	−12	30	7.6 ± 6.2	−12	30
	2	4.3 ± 7.5	−16	34	7.9 ± 7.0	−14	32
	3	1.6 ± 9.4	−18	39	7.0 ± 6.4	−18	36

Max, maximum; Min, minimum; SEMAR, single-energy metal artefact reduction.

Figure 2. Carbon-ion scanning dose distributions using head phantom images (a) without and (c) with single-energy metal artefact reduction (SEMAR). Beam spots and weights were optimized to an uncorrected image, and the dose distribution was calculated on SEMAR-corrected image (b). Dose distribution difference of (b) minus (c) is expressed by the colour scale on (d). The yellow line shows the planning target volume. For colour image see online.

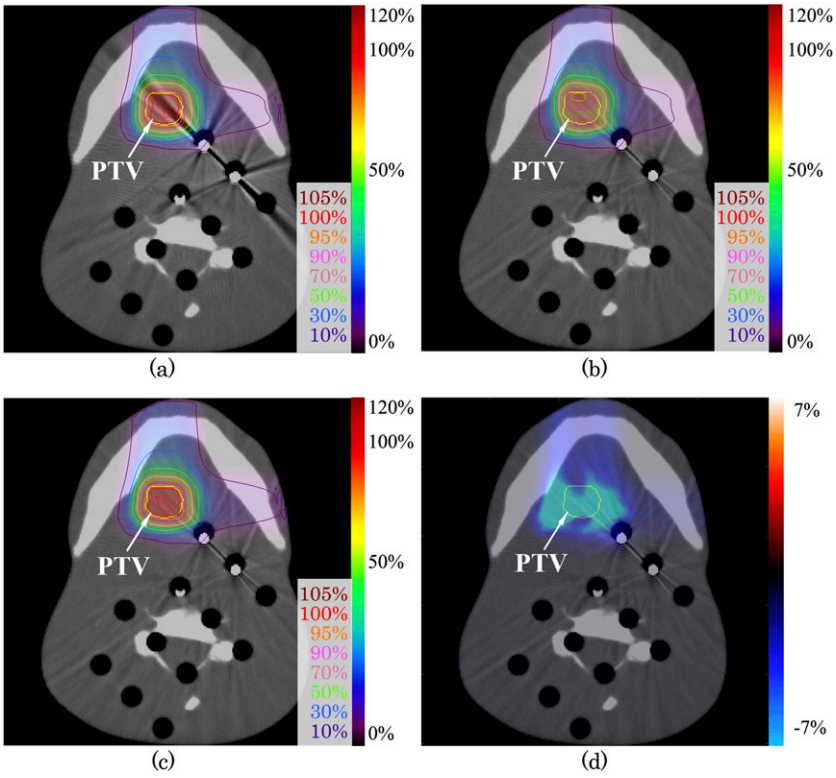

SEMAR-corrected images. The range of dose distribution differences was evaluated. Dose assessments included lowest dose delivered to 99% of volume (D_{99}), D_{95}, D_{50}, maximum dose (D_{max}) and minimum dose (D_{min}) of PTV and D_{max} of cord. To evaluate the numerical distribution difference, gamma index analysis was performed for uncorrected and SEMAR-corrected. Gamma analysis criteria of 3%/3 mm and 2%/2 mm were used for acceptable dose deviation and distance-to-agreement, respectively.

RESULTS AND DISCUSSIONS

Phantom study

The metal artefact images of head phantom without and with SEMAR are shown in Figure 1. In three metals inserted case (Figure 1c, f), the HU difference between metal-free images and metal artifact-containing images without and with SEMAR were -79.5 ± 97.2 HU and -1.4 ± 19.5 HU within ROI 1, -6.9 ± 10.9 HU and -1.5 ± 8.4 HU within ROI 2, respectively. The HU value on the uncorrected image was improved

Table 2. The range of dose difference and passing rate of gamma index analysis between uncorrected and single-energy metal artefact reduction-corrected images

	Head phantom		Patient 1		Patient 2	
	Within PTV	Whole image	Within PTV	Whole image	Within PTV	Whole image
Dose difference						
Max (%)	−3.4	0.3	1.0	4.7	2.3	11.0
Min (%)	−19.5	−24.7	−3.5	−17.0	−12.8	−17.9
Gamma analysis passing rate						
3%/3 mm (%)	–	89.1	–	100.0	–	92.7
2%/2 mm (%)	–	79.0	–	99.8	–	81.0

Max, maximum; Min, minimum; PTV, planning target volume.
Gamma analysis criteria of 3%/3 mm and 2%/2 mm (acceptable dose deviation/distance-to-agreement) were used.

Table 3. Metal artefact reduction with CT for carbon-ion therapy

Metrics	Head phantom		Patient 1		Patient 2	
	Uncorrected	SEMAR-corrected	Uncorrected	SEMAR-corrected	Uncorrected	SEMAR-corrected
PTV						
D_{99} (%)	79.4	93.1	83.9	82.9	86.3	91.0
D_{95} (%)	82.4	95.4	92.2	92.5	90.9	95.7
D_{50} (%)	91.0	99.3	99.1	99.2	98.0	99.8
D_{max} (Gy (RBE))	59.9	60.5	62.8	63.4	64.5	64.5
D_{min} (Gy (RBE))	43.2	53.0	39.2	39.2	39.2	41.5
Cord						
D_{max} (Gy (RBE))	–	–	12.7	12.1	19.8	16.7

D_{50}, dose delivered to 50% of volume; D_{95}, dose delivered to 95% of volume; D_{99}, dose delivered to 99% of volume; D_{max}, maximum irradiated dose; D_{min}, minimum irradiated dose; PTV, planning target volume; RBE, relative biological effectiveness; SEMAR, single-energy metal artefact reduction. Dose assessment results of uncorrected and SEMAR-corrected images. Uncorrected dose distribution was generated by beam plan of uncorrected images applying to SEMAR-corrected images. SEMAR-corrected dose distribution was generated by beam spots optimization to SEMAR-corrected images.

after SEMAR correction. Even, the positions far from visible metal artefact (ROI 2) were closer, in HU, to the metal-free image after SEMAR correction. SEMAR substantially improved image quality without changing HUs in the artefact-free region, though some artefacts persisted. The calculated HU values are summarized in Table 1.

Figure 3. Carbon-ion scanning dose distributions of the patient with head and neck tumour (a) without and (c) with single-energy metal artefact reduction (SEMAR) for Patient 1. Beam spots and weights were optimized to an uncorrected image, and the dose distribution was calculated on SEMAR-corrected image (b). Dose distribution difference of (b) minus (c) is expressed by the colour scale on (d). The yellow line shows the planning target volume. For colour image see online.

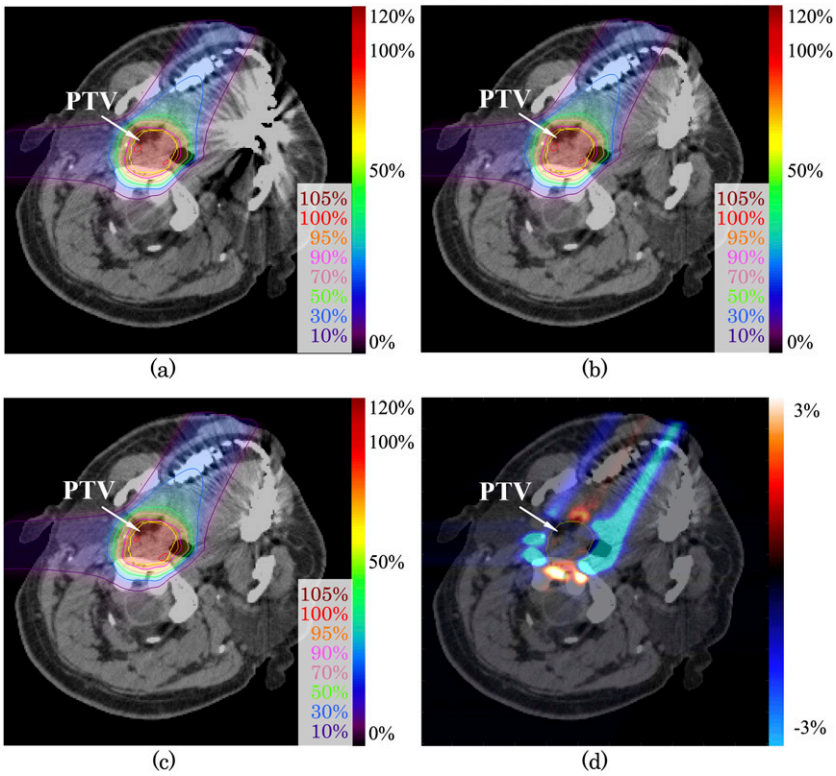

The dose distribution evaluations for a metal artefact image with and without SEMAR, and dose distribution difference of these images are shown in Figure 2. Dark artefacts around the metal screws were interpreted by the TPS as low-density materials. The range of dose distribution difference between uncorrected and SEMAR-corrected distribution was −19.5% to −3.4% from the prescribed dose within PTV and −24.7% to 0.3% for whole image (Figure 2d). The passing rate of gamma analysis with 3%/3 mm and 2%/2 mm criteria were 89.1% and 79.0%, respectively (Table 2). The PTV-D_{95} (%) for uncorrected and SEMAR-corrected images were 82.4% and 95.4%, respectively. SEMAR improved the PTV-D_{95} (%). The dose assessment results are summarized in Table 3.

Patient study

Figure 3 shows the image with metal artefact from dental implants of Patient 1. Treatment beam angle was selected across the metal artefacts. The dose distribution differences for the prescribed dose between uncorrected and SEMAR-corrected images are shown in Figure 3d. The range of dose distribution difference between uncorrected and SEMAR-corrected images was −3.5% to 1.0% from the prescribed dose within PTV and −17.0% to 4.7% for whole image. The passing rate of gamma analysis with 3%/3 mm and 2%/2 mm criteria were 99.9% and 99.8%, respectively (Table 2). The PTV-D_{95} (%) for uncorrected and SEMAR-corrected data were 92.2% and 92.5%, respectively. Although >10% of dose difference was observed, there was no significant difference on dose distribution, according to the gamma analysis. Since large differences were observed mainly peripheral to the PTV and not inside the PTV as shown in Figure 3d, SEMAR had less influence on the PTV-D_{95} (%) in this case. However, undershoot and overshoot were observed on the peripheral to the PTV. If OARs located around PTV, SEMAR could contribute the dose reduction for normal tissues. The maximum dose of cord for uncorrected and SEMAR-corrected were 12.7 Gy (RBE) and 12.1 Gy (RBE), respectively.

To study the severe case using the image of Patient 2, treatment beam was deliberately irradiated over the dental implants itself as shown in Figure 4. The range of dose distribution difference between uncorrected and SEMAR-corrected distribution was −12.8% to 2.3% from the prescribed dose within PTV and −17.9% to 11.0% for whole image. The passing rate of gamma analysis with 3%/3 mm and 2%/2 mm criteria were 92.7% and 81.0%, respectively (Table 2). The PTV-D_{95} (%) for uncorrected and SEMAR-corrected data were 90.9% and 95.7%, respectively. Owing to optimization of the beam spot and beam energy weighting for uncorrected images, the dose distribution was degraded on the image with reduced artefacts. Lin et al[31] reported the dosimetric impact of metals on volumetric-modulated arc therapy, with 0.0–3.6% differences in D_{95} observed in cases with metal artefacts, using corrected and uncorrected images. The effect of SEMAR on dose distribution depends on the location of the implant and its proximity to the PTV and OARs.

Figure 4. Carbon-ion scanning dose distributions of the patient with head and neck tumour (a) without and (c) with single-energy metal artefact reduction (SEMAR) for Patient 2. Beam spots and weights were optimized to an uncorrected image, and the dose distribution was calculated on SEMAR-corrected image (b). Dose distribution difference of (b) minus (c) is expressed by the colour scale on (d). The yellow line shows the planning target volume. For colour image see online.

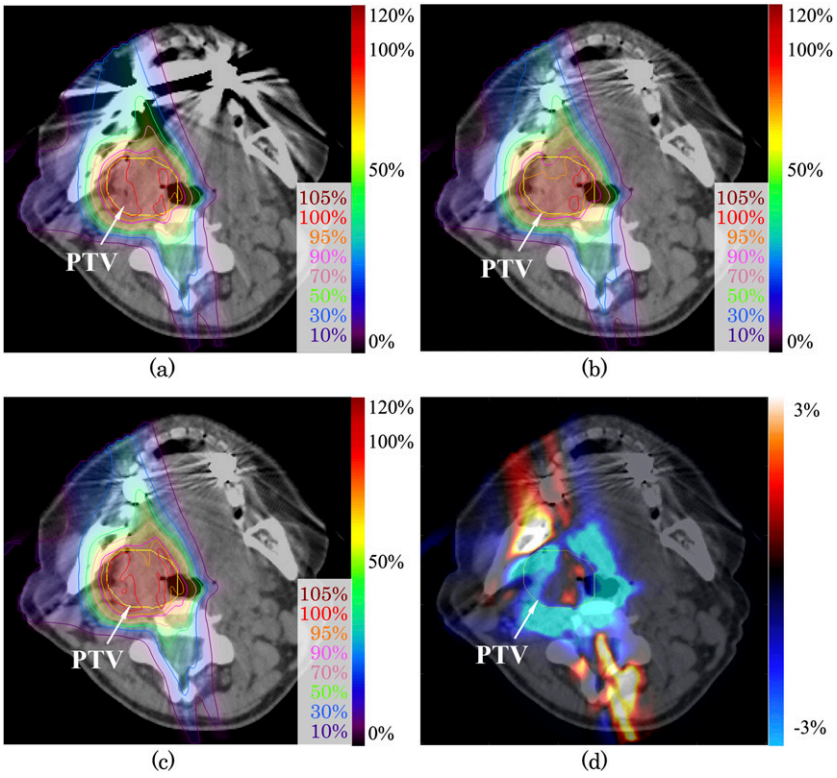

SEMAR algorithm segmented metal materials on the acquired CT images by HU threshold in the first step; therefore, it does not change any HUs to the images of metal-free object. In the case of applying SEMAR to no-screw inserted head phantom, the measured HUs of uncorrected and SEMAR-corrected images should be the same as shown in Table 1. SEMAR substantially improved image quality without changing HUs in the artefact-free objects; therefore, this algorithm can apply for metal-free patients. In this study, to compare the dose distribution degradation between beam plans of uncorrected and SEMAR-corrected images, beam spots were optimized on uncorrected image, and the dose distribution was calculated on SEMAR-corrected images using the resulting plan. We confirmed that SEMAR substantially improves image quality in the comparison of the metal-containing images and metal-free images, using head phantom. When we assumed that this improvement was reproducible in patient case, dose distribution differences between uncorrected and SEMAR-corrected in the patient study were indicative of the difference of planning dose distribution without SEMAR and actual irradiation.

The SEMAR algorithm is a raw data-based correction method which uses a single energy, giving it an advantage over dual energy or megavoltage CT in which it can generate an accurate dose distribution without any additional patient dose. As a study limitation, additional patient data sets are required before this method can be used in routine carbon-ion therapy. Although we evaluated the data sets of only two patients, our results suggest that SEMAR improves dose distribution correctly in cases with metal artefacts.

CONCLUSION

We evaluated image quality and carbon-ion dose distribution with SEMAR, using a head phantom and patient CT data. From our study, image quality and dose calculations were improved using the SEMAR algorithm. These results may contribute to the improvement of treatment accuracy without the need for dental implant extraction in patients with head and neck cancer.

REFERENCES

1. Kanematsu N, Matsufuji N, Kohno R, Minohara S, Kanai T. A CT calibration method based on the polybinary tissue model for radiotherapy treatment planning. *Phys Med Biol* 2003; **48**: 1053–64. doi: http://dx.doi.org/10.1088/0031-9155/48/8/307
2. Barrett JF, Keat N. Artifacts in CT: recognition and avoidance. *Radiographics* 2004; **24**: 1679–91. doi: http://dx.doi.org/10.1148/rg.246045065
3. Kidoh M, Nakaura T, Nakamura S, Tokuyasu S, Osakabe H, Harada K, et al. Reduction of dental metallic artefacts in CT: value of a newly developed algorithm for metal artefact reduction (O-MAR). *Clin Radiol* 2014; **69**: E11–16. doi: http://dx.doi.org/10.1016/j.crad.2013.08.008
4. Haberer T, Debus J, Eickhoff H, Jakel O, Schulz-Ertner D, Weber U. The heidelberg ion therapy center. *Radiother Oncol* 2004; **73**: S186–S90. doi: http://dx.doi.org/10.1016/S0167-8140(04)80046-X
5. Bamberg F, Dierks A, Nikolaou K, Reiser MF, Becker CR, Johnson TR. Metal artifact reduction by dual energy computed tomography using monoenergetic extrapolation. *Eur Radiol* 2011; **21**: 1424–29. doi: http://dx.doi.org/10.1007/s00330-011-2062-1
6. De Marzi L, Lesven C, Ferrand R, Sage J, Boule T, Mazal A. Calibration of CT Hounsfield units for proton therapy treatment planning: use of kilovoltage and megavoltage images and comparison of parameterized methods. *Phys Med Biol* 2013; **58**: 4255–76. doi: http://dx.doi.org/10.1088/0031-9155/58/12/4255
7. Paudel MR, Mackenzie M, Fallone BG, Rathee S. Clinical evaluation of normalized metal artifact reduction in kVCT using MVCT prior images (MVCT-NMAR) for radiation therapy treatment planning. *Int J Radiat Oncol Biol Phys* 2014; **89**: 682–89. doi: http://dx.doi.org/10.1016/j.ijrobp.2014.02.040
8. Wang G, Snyder DL, Osullivan JA, Vannier MW. Iterative deblurring for CT metal artifact reduction. *IEEE Trans Med Imaging* 1996; **15**: 657–64. doi: http://dx.doi.org/10.1109/42.538943
9. De Man B, Nuyts J, Dupont P, Marchal G, Suetens P. Reduction of metal streak artifacts in X-ray computed tomography using a transmission maximum a posteriori algorithm. *IEEE Trans Nucl Sci* 2000; **47**: 977–81. doi: http://dx.doi.org/10.1109/23.856534
10. Meyer E, Raupach R, Lell M, Schmidt B, Kachelriess M. Frequency split metal artifact reduction (FSMAR) in computed tomography. *Med Phys* 2012; **39**: 1904–16. doi: http://dx.doi.org/10.1118/1.3691902
11. Kalender WA, Hebel R, Ebersberger J. Reduction of CT artifacts caused by metallic implants. *Radiology* 1987; **164**: 576–77. doi: http://dx.doi.org/10.1148/radiology.164.2.3602406
12. Abdoli M, Ay MR, Ahmadian A, Dierckx R, Zaidi H. Reduction of dental filling metallic artifacts in CT-based attenuation correction of PET data using weighted virtual sinograms optimized by a genetic algorithm. *Med Phys* 2010; **37**: 6166–77. doi: http://dx.doi.org/10.1118/1.3511507
13. Zhao SY, Bae KT, Whiting B, Wang G. A wavelet method for metal artifact reduction with multiple metallic objects in the field of view. *J Xray Sci Technol* 2001; **10**: 67–76.
14. Zhang Y, Pu YF, Hu JR, Liu Y, Zhou JL. A new CT metal artifacts reduction algorithm based on fractional-order sinogram inpainting. *J Xray Sci Technol* 2011; **19**: 373–84. doi: http://dx.doi.org/10.3233/XST-2011-0300
15. Mehranian A, Ay MR, Rahmim A, Zaidi H. X-ray CT metal artifact reduction using wavelet domain L-0 sparse regularization. *IEEE Trans Med Imaging* 2013; **32**: 1707–22. doi: http://dx.doi.org/10.1109/TMI.2013.2265136
16. Mehranian A, Ay MR, Rahmim A, Zaidi H. 3D prior image constrained projection completion for X-ray CT metal artifact reduction. *IEEE Trans Nucl Sci* 2013; **60**: 3318–32. doi: http://dx.doi.org/10.1109/TNS.2013.2275919
17. Gondim Teixeira PA, Meyer JB, Baumann C, Raymond A, Sirveaux F, Coudane H, et al. Total hip prosthesis CT with single-energy projection-based metallic artifact reduction: impact on the visualization of specific periprosthetic soft tissue structures. *Skeletal Radiol* 2014; **43**: 1237–46. doi: http://dx.doi.org/10.1007/s00256-014-1923-5
18. Funama Y, Taguchi K, Utsunomiya D, Oda S, Hirata K, Yuki H, et al. A newly-developed metal artifact reduction algorithm improves the visibility of oral cavity lesions on 320-MDCT volume scans. *Phys Med* 2015; **31**: 66–71. doi: http://dx.doi.org/10.1016/j.ejmp.2014.10.003

19. Nawaz S, Fu J, Fan D. Metal artifacts reduction in X-ray CT based on segmentation and forward-projection. *Biomed Mater Eng* 2014; **24**: 3287–93. doi: http://dx.doi.org/10.3233/BME-141151
20. Bal M, Spies L. Metal artifact reduction in CT using tissue-class modeling and adaptive prefiltering. *Med Phys* 2006; **33**: 2852–59. doi: http://dx.doi.org/10.1118/1.2218062
21. Willemink MJ, de Jong PA, Leiner T, de Heer LM, Nievelstein RAJ, Budde RPJ, et al. Iterative reconstruction techniques for computed tomography part 1: technical principles. *Eur Radiol* 2013; **23**: 1623–31. doi: http://dx.doi.org/10.1007/s00330-012-2765-y
22. Willemink MJ, Leiner T, de Jong PA, Heer LM, Nievelstein RA, Schilham AM, et al. Iterative reconstruction techniques for computed tomography part 2: initial results in dose reduction and image quality. *Eur Radiol* 2013; **23**: 1632–42. doi: http://dx.doi.org/10.1007/s00330-012-2764-z
23. Gervaise A, Osemont B, Lecocq S, Noel A, Micard E, Felblinger J, et al. CT image quality improvement using adaptive iterative dose reduction with wide-volume acquisition on 320-detector CT. *Eur Radiol* 2012; **22**: 295–301. doi: http://dx.doi.org/10.1007/s00330-011-2271-7
24. Inaniwa T, Kanematsu N, Matsufuji N, Kanai T, Shirai T, Noda K, et al. Reformulation of a clinical-dose system for carbon-ion radiotherapy treatment planning at the National Institute of Radiological Sciences, Japan. *Phys Med Biol* 2015; **60**: 3271–86. doi: http://dx.doi.org/10.1088/0031-9155/60/8/3271
25. Inaniwa T, Kanematsu N, Hara Y, Furukawa T. Nuclear-interaction correction of integrated depth dose in carbon-ion radiotherapy treatment planning. *Phys Med Biol* 2015; **60**: 421–35. doi: http://dx.doi.org/10.1088/0031-9155/60/1/421
26. Inaniwa T, Kanematsu N. A trichrome beam model for biological dose calculation in scanned carbon-ion radiotherapy treatment planning. *Phys Med Biol* 2015; **60**: 437–51. doi: http://dx.doi.org/10.1088/0031-9155/60/1/437
27. Inaniwa T, Kanematsu N, Hara Y, Furukawa T, Fukahori M, Nakao M, et al. Implementation of a triple Gaussian beam model with subdivision and redefinition against density heterogeneities in treatment planning for scanned carbon-ion radiotherapy (vol 59, pg 5361, 2014). *Phys Med Biol* 2014; **59**: 6305–05. doi: http://dx.doi.org/10.1088/0031-9155/59/20/6305
28. Inaniwa T, Furukawa T, Kanematsu N, Mori S, Mizushima K, Sato S, et al. Evaluation of hybrid depth scanning for carbon-ion radiotherapy. *Med Phys* 2012; **39**: 2820–25. doi: http://dx.doi.org/10.1118/1.4705357
29. Inaniwa T, Furukawa T, Tomitani T, Sato S, Noda K, Kanai T. Optimization for fast-scanning irradiation in particle therapy. *Med Phys* 2007; **34**: 3302–11. doi: http://dx.doi.org/10.1118/1.2754058
30. Kanai T, Endo M, Minohara S, Miyahara N, Koyama-Ito H, Tomura H, et al. Biophysical characteristics of HIMAC clinical irradiation system for heavy-ion radiation therapy. *Int J Radiat Oncol Biol Phys* 1999; **44**: 201–10. doi: http://dx.doi.org/10.1016/S0360-3016(98)00544-6
31. Lin MH, Li J, Price RA Jr, Wang L, Lee CC, Ma CM. The dosimetric impact of dental implants on head-and-neck volumetric modulated arc therapy. *Phys Med Biol* 2013; **58**: 1027–40. doi: http://dx.doi.org/10.1088/0031-9155/58/4/1027